

Article

Investigation of Lips-Guided-Flow Combustion Chamber and Miller Cycle to Improve the Thermal Efficiency of a Highly Intensified Diesel Engine

Ziyu Wang ¹, Rulou Cao ¹, Yanfang Li ¹, Caifeng Hao ¹, Jinlong Liu ¹, Yanzhao An ^{2,*} and Renwei Ma ³¹ China North Engine Research Institute, Tianjin 300400, China² State Key Laboratory of Engines, Tianjin University, Tianjin 300072, China³ Jinkang New Energy Power Co., Ltd., Chongqing 401333, China

* Correspondence: yanzhao_an@tju.edu.cn

Abstract: An investigation into the lips-guided-flow combustion chamber (LGFC) and Miller cycle was conducted on a highly intensified diesel engine under rated power conditions to improve thermal efficiency. The radius and depth of the chamber bowl and lips were optimized to intensify the guided flow and fuel/air mixing. The experimental and simulated results show that the LGFC had a higher fuel/air mixture quality and quicker combustion rate, leading to a higher indicated power and higher thermal efficiency. A late intake valve closing (LIVC) Miller cycle with a higher expansion ratio of 11 and a lower compression ratio of 8.2 was used to control the energy distribution of the thermodynamic cycle and reduce the mechanical and thermal loads. The results show that the maximum combustion temperature was decreased by about 45 K and the thermal efficiency was improved by 2.1%. The research results are useful to guide the improvement in thermal efficiency through combustion chamber design and Miller cycle application for highly intensified diesel engines.

Keywords: highly intensified diesel engine; lips-guided-flow combustion chamber; Miller cycle; thermal efficiency



Citation: Wang, Z.; Cao, R.; Li, Y.; Hao, C.; Liu, J.; An, Y.; Ma, R. Investigation of Lips-Guided-Flow Combustion Chamber and Miller Cycle to Improve the Thermal Efficiency of a Highly Intensified Diesel Engine. *Sustainability* **2023**, *15*, 14968. <https://doi.org/10.3390/su152014968>

Academic Editor: Luca Cioccolanti

Received: 15 August 2023

Revised: 30 September 2023

Accepted: 10 October 2023

Published: 17 October 2023



Copyright: © 2023 by the authors. Licensee MDPI, Basel, Switzerland. This article is an open access article distributed under the terms and conditions of the Creative Commons Attribution (CC BY) license (<https://creativecommons.org/licenses/by/4.0/>).

1. Introduction

Highly intensified diesel engines have received increasing attention in recent years as they are effective in dealing with the stringent standards on vehicle emissions and fuel consumption [1–6]. A highly intensified power output can be achieved by increasing the power density and increasing the engine speed. Increasing power density requires the burning of a large amount of fuel in a short combustion period. The fuel/air mixing process has to be significantly intensified as the combustion rate depends on the fuel/air mixing rate in diesel engines. Increasing engine speed leads to a significant decrease in volumetric efficiency, especially under a swirling flow condition. Furthermore, a reduced excess air ratio is often required in order to reduce the size of the air supply system.

All these requirements could lead highly intensified diesel engines to experience incomplete combustion and less thermal efficiency, but higher thermal, mechanical loads, etc. [4,5,7]. In order to improve the thermal efficiency and reduce the thermal and mechanical loads, technical measures must be taken to intensify the combustion process and actively control the energy distribution during a cycle. The combustion chamber design and Miller cycle intake timing are two of the most effective measures and have been extensively studied.

The combustion chamber significantly influences the combustion process by intensifying the in-cylinder fuel/air mixing and the near-wall flow field, which makes it one of the most important aspects for optimizing the energy distribution in diesel engines. HAO et al. [7] investigated the combustion chamber geometry and its interaction with

the spray angle in a heavy-duty diesel engine to improve combustion performance under full-load conditions. A sensitivity analysis of the effects of the stepped-lip chamber geometry parameters on fuel/air mixing and combustion process was carried out using computational fluid dynamics (CFD) modeling. The simulated results showed that the stepped-lip combustion chamber had a great influence on the combustion process in a heavy-duty diesel engine. A larger lip radius changed the position of the vortex center of the high spray in the combustion chamber to close to the center of the cylinder and had a larger distribution area, which could improve the quality of the fuel/air mixture. The bowl radius, bowl distance, and lip depth were the other important optimization parameters. CHEN et al. [8] designed a lateral-swirl combustion system (LSCS) to promote spatial spray distribution (in Figure 1). In the LSCS combustion system, a split edge was designed on the wall of the chamber in the direction of each injection hole, and the fuel spray was divided into two bundles after colliding with the split edge, and two sets of lateral convolutions were formed in the combustion chamber. The numerical and experimental results proved that the spray impingement positions of the LSCS must be precisely on the corresponding convex edges of the chamber, and the combustion system gained the best combustion performance attributed to its fullest wall flow guidance provided by the unique geometric shape of the chamber. The results showed that the optimized chamber geometry could achieve better smoke emissions and higher thermal efficiency, improved utilization rate of the circumferential air in the combustion chamber, reduced fuel accumulation on the cylinder wall, and better fuel/air mixture. As a result, the combustion system increased the indicated power and decreased the soot mass fraction in the high-speed direct-injection diesel engine. LI et al. [9,10] designed and studied a forced swirl combustion system (FSCS) and multi-swirl combustion system (MSCS). The improvement of the fuel/air mixture formation of FSCS was conducted for the combustion and emission characteristics of FSCS to reveal the differences and relations among fuel/air diffusion, in-cylinder velocity distribution, turbulent kinetic energy, in-cylinder temperature distribution, and emissions between FSCS and traditional omega combustion system (OMECS) by CFD. The results showed that the fuel/air mixing promotion and emission of DI diesel engines were both improved in the FSCS system [9]. In the MSCS system, after the fuel spray touched the circular ridge, two swirls formed in opposing directions in the longitudinal space, and during the injection process, the fuel in the outer chamber touched the convex edge and formed two lateral swirls. It is concluded that the multi-swirl accelerated the fuel diffusion over the entire chamber, rendering the fuel/air mixture more uniform and improving the utilization of the air in the combustion chamber [10]. The results showed that the two systems accelerated fuel/air mixing and improved the combustion process by increasing the flow conductivity of the combustion chamber.

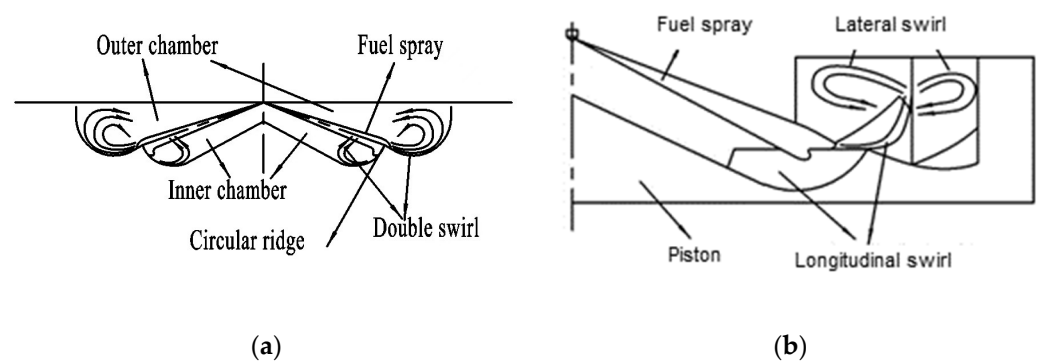


Figure 1. The schematic diagrams of different combustion systems [9]. (a) The schematic diagram of FSCS. (b) The schematic diagram of MSCS.

In summary, with the demand for higher power density in diesel engines, the engine speed and cycle fuel injection have increased at the same time, which means that more fuel is injected into the cylinder at the same time, and fuel atomization must be enhanced.

Therefore, the guided-flow combustion chamber was optimized to enhance the squeezing effect of the piston moving, which improved the quality of the fuel/air mixture and reduced the combustion period [5,11–13].

The Miller cycle, which has recently been widely applied to passenger cars and ships, is an effective solution for improving the thermal efficiency of gasoline engines and low-speed diesel engines [14]. The expansion ratio of the engine is larger than the compression ratio (CR) under the Miller cycle by making the intake valves close (IVC) before or after the bottom dead center, thereby improving thermal efficiency [14–16]. A thermodynamic analysis of a Miller cycle gasoline engine with early intake valve closing (EIVC) was conducted by CHEN et al. [16]. They proposed a novel approach to an electrically supercharged Miller cycle with EIVC based on thermodynamics to settle the fuel economy problem of gasoline engines. The results showed that the Miller cycle with EIVC could reduce pumping and exhaust losses by dominating intake air and over-expanding the working medium, which led to the energy flow of the electrically supercharged Miller cycle engine with EIVC improving the thermal efficiency substantially. The mechanism is that the application of an electrically supercharged Miller cycle with EIVC increases air pressure, which leads to notably decreased pumping loss, while the reduction in pumping loss increases with the increase in speeds and loads. The increment in the in-cylinder temperature could also decrease exhaust loss. Eventually, the heat transfer and friction losses slightly increased, while the increase exerted a trivial effect on the thermal efficiency. DUMBOCK et al. [17] discussed the extended expansion theory of the Miller cycle. Measurements and simulations revealed that, considering mechanical issues, such as friction and mass balancing, it may be more convenient to use the Miller cycle process in a short-term series solution to increase efficiency. The results showed that a Miller cycle with an expansion ratio γ of 2 achieved an efficiency improvement of seven percentage points compared with a conventional crank train engine. It was also found that the extended expansion had no inherent effect on the combustion process, emissions, and wall heat transfer. The Miller cycle could suffer in a way from higher wall heat and gas exchange losses, cutting a substantial share of the efficiency potential of an equivalent crank train solution. WEI et al. [18] aimed to control the energy distribution of the thermodynamic cycle with combustion chamber geometries, and the Miller cycle was investigated on a highly intensified diesel engine to improve the thermal efficiency, and studied the effects of the EIVC Miller cycle on the combustion and emissions of marine diesel engines by the CFD model. The simulation results showed that the in-cylinder pressure, temperature, and NO emissions were reduced under EIVC conditions. ZHANG et al. [19] also used the Miller cycle to improve the combustion of a highly intensified single-cylinder diesel engine to achieve a nearly ideal thermodynamic cycle. The engine test result showed that, when the late intake valve closing (LIVC) timing was decreased from the original 70° crank angle (CA) after bottom dead center (ABDC) to 120° CA ABDC, the peak combustion pressure and the peak combustion temperature were presently decreased under 3600 r/min operating conditions. As the LIVC timing decreased, the intake pressure increased noticeably in order to maintain the intake air mass and the engine power output, leading to a noticeable change in charging efficiency, pumping loss, and exhaust energy. The results showed that under the Miller cycle with LIVC condition, on the one hand, the effective compression ratio in the cylinder was decreased by 5.1 and the expansion ratio remained the same (about 11) to form a thermal cycle of short compression and large expansion. The in-cylinder temperature and cylinder pressure at the compression stroke end became lower so that the start of combustion (SOC) could be advanced to enhance the constant volume degree of in-cylinder combustion, which is the main way to increase the efficiency of diesel engines [20–22]. Under the same power output condition, the maximum combustion temperature, peak pressure, and exhaust temperature decreased. On the other hand, with the delay in the intake valve close timing, pump pressure was higher and pump work became positive. As shown in Figure 2, the combined effects of the two aspects increased the thermal efficiency of highly intensified diesel engines.

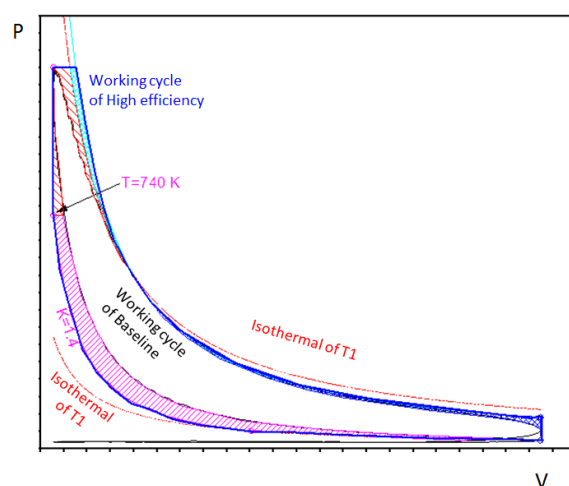


Figure 2. Nearly ideal thermodynamic cycle and practical working cycle of a highly intensified diesel engine.

KOVACS et al. [23] investigated the Miller loss on a high-load diesel engine running with the LIVC Miller strategy. The results showed that the intake pressure had to be increased to obtain enough charge quantity at different LIVCs, resulting in a higher Miller loss due to the delayed start of compression.

As reviewed above, the combustion chamber geometry and Miller cycle have a major effect on combustion performance and thermal efficiency. In this study, the combustion chamber geometries and Miller cycle were investigated on a highly intensified single-cylinder diesel engine to improve the thermal efficiency through the following three steps: (1) to optimize the combustion quality and phase by LGFC combustion chamber design, (2) to extend the expansion process by the LIVC Miller cycle, and (3) to reduce the pumping loss and the heat transfer loss by combining the optimized combustion chamber and the LIVC Miller cycle. The working process was studied through experiments and simulations. The effects of the in-cylinder flow and combustion process were analyzed.

2. Experiment and Simulation

2.1. Combustion Chamber Design

In order to optimize the combustion chamber, some typical parameters of the lips-guided-flow combustion chamber were defined, as shown in Figure 3, and their values were determined by bench experiment and CFD simulation. Table 1 provides the chamber parameters determined versus the original chamber geometry. In the LGFC combustion system, a specially designed geometry increases the crushing strength, which is caused by the decreasing chamber radius and bowl distance, and the increasing lip depth and bowl radius (see Figure 4 and Table 1). Based on the traditional ω combustion system (Baseline), most of the injection spray was contained within the combustion chamber by reducing the chamber radius, the effect of wall guided-flow was reinforced by increasing the lip depth, and the larger bowl radius increased the intensity of local eddies in the LGFC system.

Table 1. The chamber parameters of the baseline and LGFC.

Chamber Parameters	Baseline	LGFC
Chamber radius (mm)	44	41.5
Lips radius (mm)	36.05	36
Lips depth (mm)	4	5.5
Bowl radius (mm)	4.5	5
Bowl distance (mm)	33	32

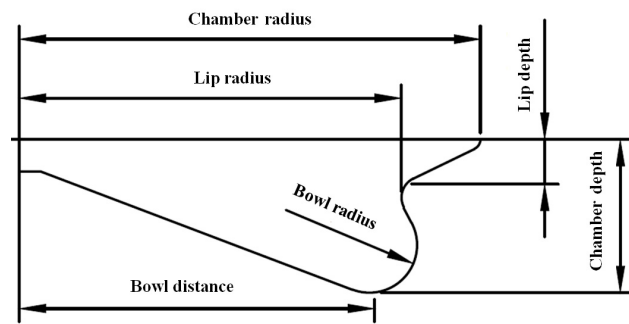


Figure 3. Combustion chamber geometry parameters.

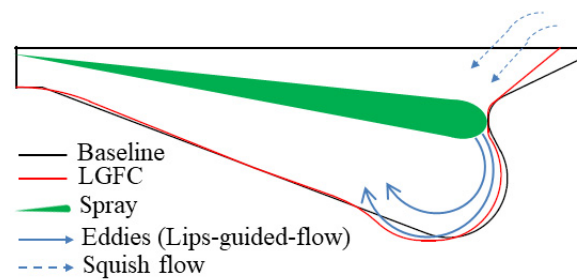


Figure 4. Combustion chamber phases of the baseline and LGFC.

2.2. LIVC Miller Cycle

The intake and exhaust valve timings used for the Miller cycle test in this work are illustrated in Figure 5, in which the baseline valve timing profile is also plotted. The maximum valve lift was 8 mm. The exhaust valve timing was maintained throughout the tests, while the intake camshaft was changed to run the Miller cycle. In the baseline, the IVC timing was 70° CA ABDC. The LIVC Miller camshafts were designed with the same rising profile as the original camshaft, but holding longer in the maximum lift period so that the closing timing was slowed to 94° CA ABDC.

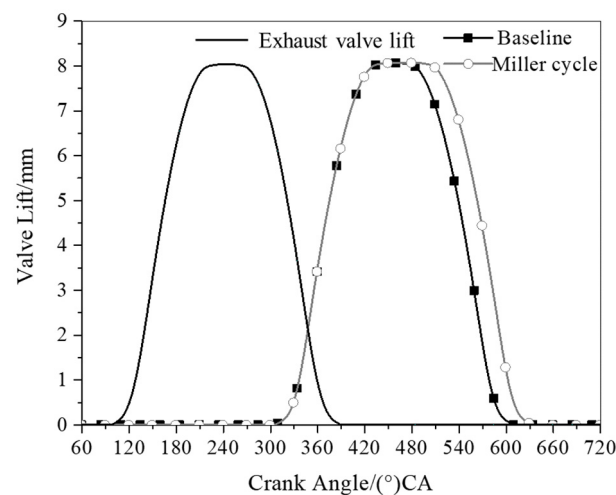


Figure 5. Valve life curves of the baseline and Miller cycles.

Owing to the slowing of the IVC timing, the ECR (effective compression ratio) was reduced. The ECR based on the cylinder volume at the IVC timing can be calculated by the following equation [19,24].

$$ECR = \frac{V_{IVC} + V_c}{V_c} \quad (1)$$

where V_c is the chamber volume at the end of the compression stroke and V_{IVC} is the cylinder volume at the IVC timing. The IVC timing was slowed from 70° CA ABDC to 94° CA ABDC and the ECR was reduced from 11 to 8.2, nearly 75% of the original value.

In the CFD model of the Miller Cycle, it changed the intake valve life curves (IVC was 94° CA ABDC), and the initial conditions and boundary conditions were modified according to the results of the one-dimensional calculation.

2.3. Experimental Setup

The test was carried out on a highly intensified diesel engine, and the single-cylinder engine test system is shown in Figure 6. The main specifications of the engine are shown in Table 2. The diesel fuel was supplied through a common rail system with a rail pressure of 180 MPa. The high-pressure pump was actuated by an external driving system, and there were 10 holes on the nozzle of the injector, which was installed in the central axis of the combustion chamber. The compressed air was supplied by a supercharger, which was located in another building and driven by an electric motor, and cooled by an individual cooling module that was set between the supercharger and the intake ports of the diesel engine. The compressed air could be adjusted by a pre-set boost pressure. The compressed air flowed into the first surge tank in which an electrical heater was installed to control the intake air temperature through the closed-loop control of the heater. The intake air flow was measured by a mass flowmeter. Then, the compressed air moved into the second surge tank, where the intake temperature was measured. On the exhaust side, there was a cone valve before an exhaust stable pressure tank to simulate the exhaust back pressure caused by the turbocharger. The pressure/temperature of the intake pipe and the pressure/temperature of the exhaust pipe could be measured. The exhaust gas emissions were measured by an AVL exhaust gas analyzer. The instantaneous cylinder pressure was measured by a Kistler piezo-electric pressure transducer with a sampling resolution of 0.5° CA [19,24]. The specifications and properties of the test devices are shown in Table 3.

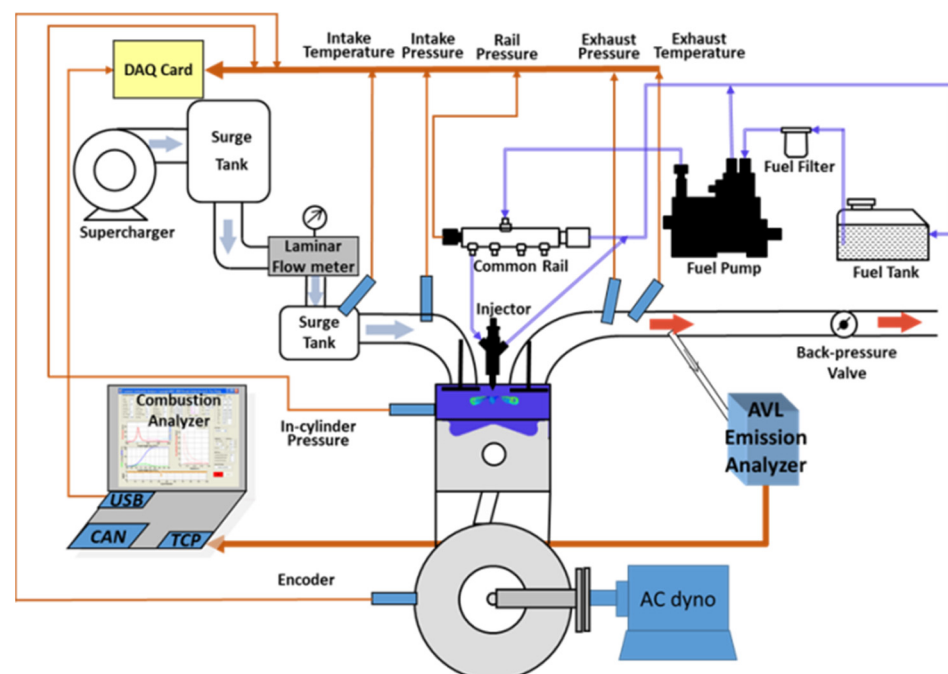


Figure 6. Schematic of the single-cylinder highly intensified diesel engine test rig.

Table 2. Engine main specifications.

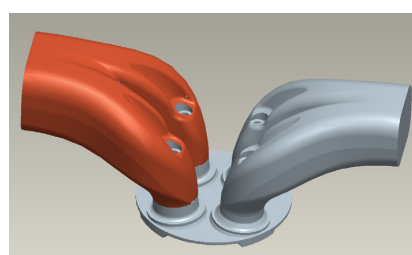
Item	Parameter
Type	Vertical, 1 cylinder, 4 stroke
Swept Volume/L	1.1
Engine Speed/rpm	3800
Compression Ratio	13:1 (Geometric)
Combustion Chamber	ω chamber
Fuel Injection System	Common Rail
Rail Pressure/MPa	180
Supercharging System	Simulated supercharging system with air compressor and heat exchanger
Valve Train	Double Overhead Camshafts
Valve Lift	See Figure 4
Number of Valves	4
Coolant Temperature/ $^{\circ}$ C	75
Fuel	Standard Diesel

Table 3. Main specifications and properties of devices.

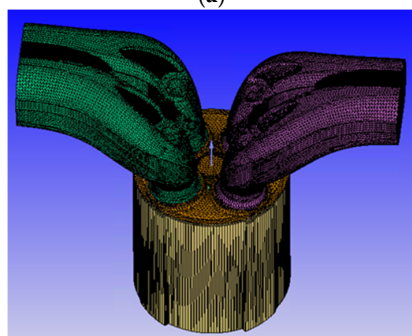
Devices	Types/Specification	Properties
Dynamometer	Electric dynamometer	0~200 kW, 0~4500 r/min, ± 1 r/min
Fuel consumption meter	Weigh-in fuel consumption meter	0.3~120 L/h, $\pm 0.2\%$
Exhaust gas analyzer	MEXA-584L	$0\sim 5 \times 10^{-3}$ (NO_x)
Mass flow meter	Sensyflow P	0~1200 m^3/h , $< 1\%$ FS
Piezo-electric pressure transducer	Kistler 6061C	0~25 MPa

2.4. Combustion and Finite Element Simulation

The combustion simulation model was built based on the test engine and CONVERGE code. The combustion chamber and charge exchange ports of the single-cylinder highly intensified diesel engine were set up and configured as a CFD modeling program, as shown in Figure 7.



(a)



(b)

Figure 7. Geometry model and STL file of the combustion chamber. (a) CAD model. (b) STL file.

To ensure the calculation accuracy and improve the calculation speed, the simulation model adopted the basic grids and local encryption method. The basic grid size was 4 mm. Automatic encryption produced 1/3 times the basic grid size according to the gradient of temperatures and velocity. The areas of automatic encryption included the spray development area during fuel injection and the valve area during valve movement. The total number of meshes was not larger than 1.2 million. In the CFD model, the flow equation was the RNG k- ϵ turbulence equation, the breakup model was KH-RT, the evaporation model was Frossling, and the combustion model was SAGE. Table 4 lists the sub-models and mechanisms of the simulation [25,26].

Table 4. Sub-models and mechanisms of the simulation.

Model Category	Sub-Models
Flow	RNS fluid control equation RNG k- ϵ turbulence equation Redlich–Kwong real gas equation
Spray	Liquid.dat variable fuel properties KH-RT breakup model NTC droplet collision model O'Rourke Turbulent Dispersion model Dynamic drop drag model Frossling evaporation model Wall film model
Combustion	SAGE combustion model

The combustion process of the Miller cycle was studied by CFD. The initial conditions and boundary conditions in the simulated model were obtained by experiments and one-dimensional simulations. The surface temperatures of the cylinder head, cylinder liner, and piston were adopted according to the empirical values of 523 K, 433 K, and 553 K, respectively.

In order to verify the CFD model, the pressure data in the cylinder were obtained under a heavy-duty condition in which the engine speed was 3600 r/min and IMEP was 2.5 MPa, and the results are shown in Figure 8. The curve trends of the experimental value and the three-dimensional calculated value were similar for the baseline, there was a certain difference between SOC and the crank angle of the maximum combustion pressure of the simulated value was slightly higher than the experimental value, and the post-combustion pressure was slightly higher than the experimental value; this means that the simulated combustion process was slightly slower than the experimental combustion process. This might be caused by the precision of the controlling parameters or leakage from rings. In addition, some of the initial conditions and boundary conditions used in the model were experimental values, which also affected the simulation results. But, in general, the differences between the experimental result and simulated result were less than 5%, and the result of the three-dimensional simulation was acceptable.

The engine test was carried out under the intake valve closing time (70° CA ABDC) of the baseline. In the CFD model of the Miller Cycle, the intake valve life curves (IVC was 94° CA ABDC) were changed, and the initial conditions and boundary conditions were modified according to the results of one-dimensional calculation.

In order to calculate the temperatures of the piston top surfaces, the piston geometric models of the baseline and LGFC were established as shown in Figure 9. Screw holes and pin holes were removed to improve the quality of the meshes. As shown in Figure 10, the mesh type was set to DC3D10 to suit the simulation of the temperature field. As finite element models do not require high-quality meshes, the mesh type was set to a tetrahedral mesh. Referring to reference [27], the thermal boundary conditions were calculated in CFD, including the temperatures of the piston top and the corresponding heat transfer coefficient. The boundary conditions of the piston side were based on data from reference [28].

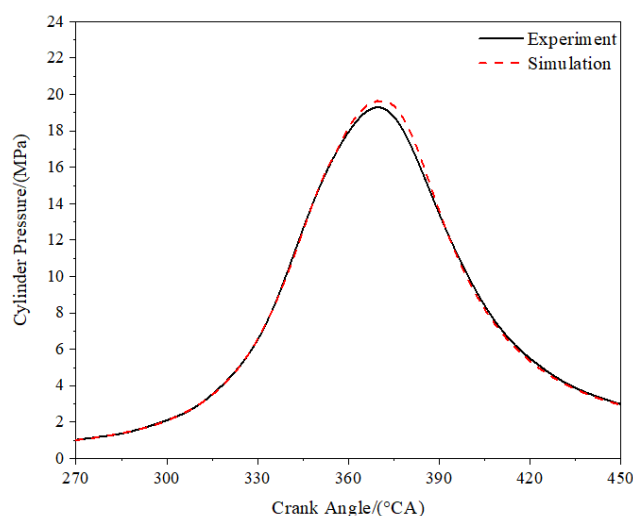


Figure 8. Experimental and simulated results of Baseline.



Figure 9. Structures of piston bodies. (a) Baseline. (b) LGFC.

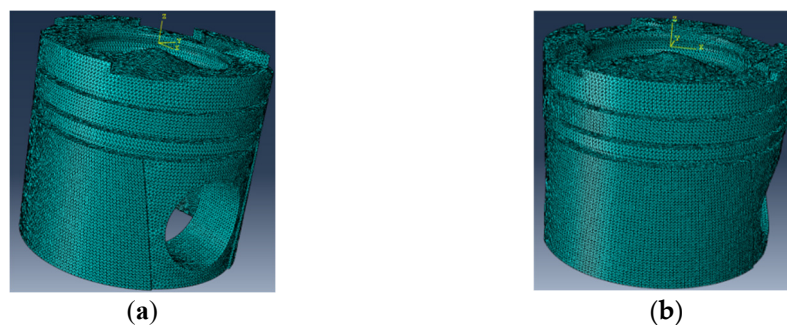


Figure 10. Finite element meshes of piston bodies. (a) Baseline. (b) LGFC.

3. Results and Discussion

3.1. LGFC Analysis

The effect of the LGFC combustion chamber was studied through the CFD model under the rated conditions, in which the engine speed was 3800 r/min and the indicated mean effective pressure (IMEP) was 3 MPa. Compared with the baseline combustion chamber, the optimized LGFC chamber exhibited stronger guided flow produced by the lips of the bowl. The extrusion flow promoted the utilization of the circumferential air of the piston for better mixing. As shown in Figure 11, the inner flow toward the chamber center along the bowl surface enhanced the mixing inside the bowl, so the area with a high fuel/air equivalence ratio under the LGFC system was larger than that of the baseline, at -10° CA after top dead center (ATDC), causing a reduction in the temperature gradient in the cross-section from the center to the cylinder wall. A larger flow structure was easily formed in the cavity of the chamber due to the large longitudinal space area, and the fuel

distribution in the cylinder was concentrated in the longitudinal direction, along with the movement of the piston. At the top dead center (TDC), the fuel/air equivalence ratio of the outside area of the piston top under the LGFC system was lower than the baseline and the combustion was more concentrated in the bowl, but less in the outside area of the piston top. The heat release rates of the baseline and the LGFC are shown in Figure 12. It can be seen that the SOC was slightly earlier under the LGFC system, the heat release rate became much higher during the best combustion phase of 0–20° CA ATDC and lower during the late combustion stage of 40–50° CA ATDC.

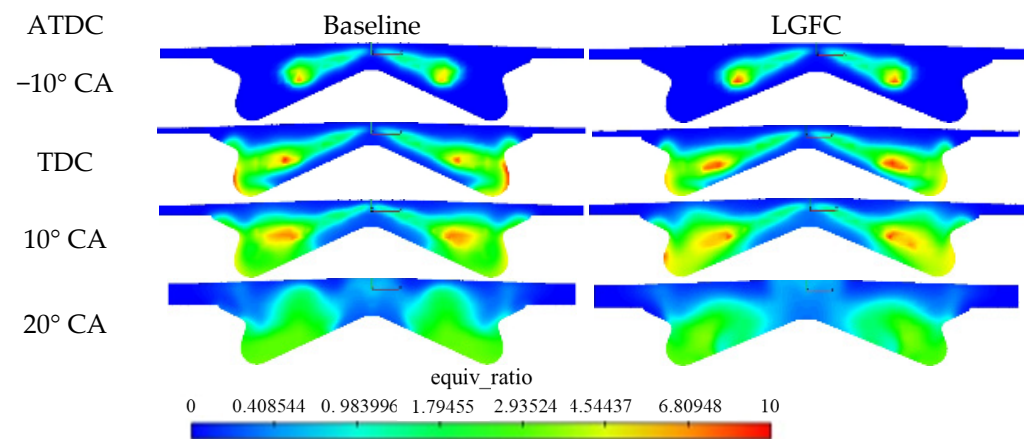


Figure 11. Fuel/air equivalence ratio of Baseline and LGFC.

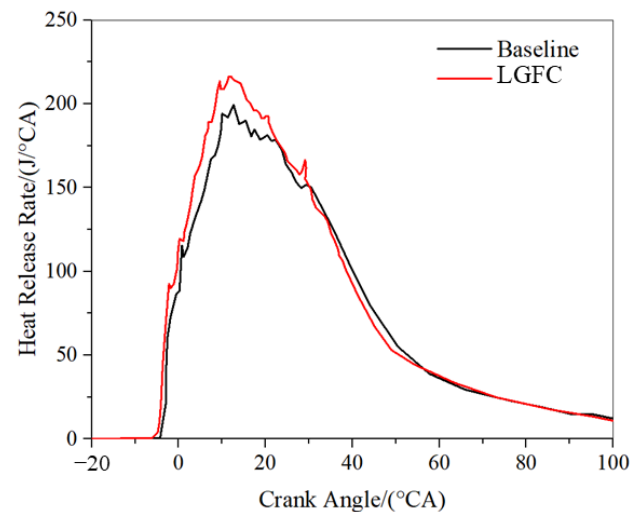


Figure 12. HRR of baseline and LGFC.

The fluid average temperature near the wall surface and the heat transfer coefficient of the piston top for both cases of the baseline and LGFC combustion chamber are shown in Figure 13. It can be seen that the high-temperature region in the LGFC case was mainly concentrated in the piston bowl, and the total areas of the high-temperature region in the LGFC case were smaller than those of the baseline case. In the LGFC case, the average heat transfer coefficient decreased and became more balanced, with the areas of high heat transfer coefficient concentrating near the lips, exactly where the sprays hit the wall. This indicates that the losses of heat transfer were suppressed.

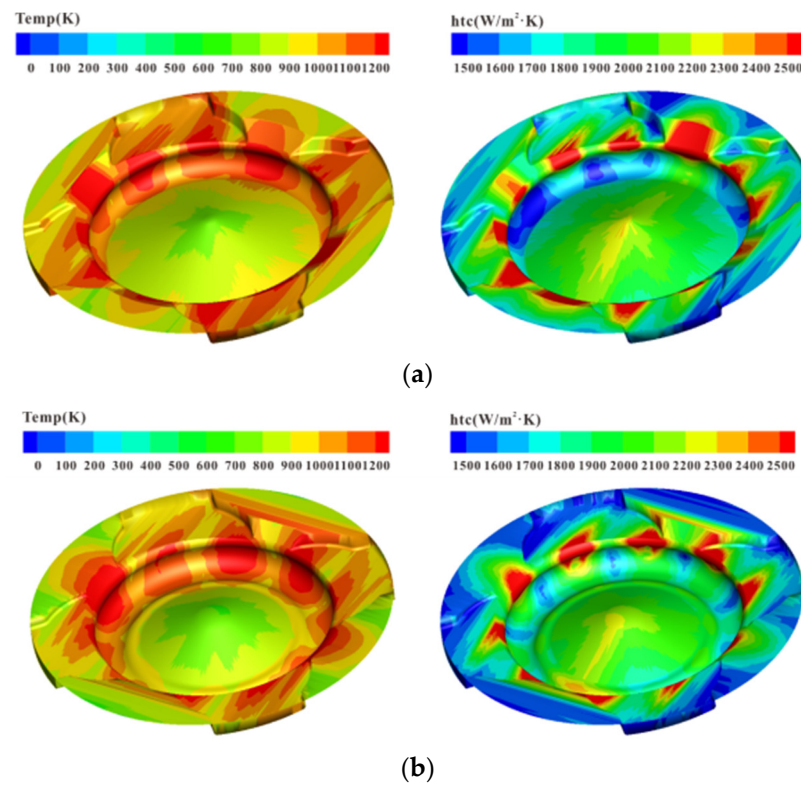


Figure 13. Fluid temperature near the wall surface and heat transfer coefficient of the piston top of the baseline and LGFC. (a) Baseline. (b) LGFC.

The average temperature distribution of the piston of the baseline and LGFC is shown in Figure 14. The simulation results show that the maximum temperature of the baseline and LGFC were 651 K and 636 K, respectively, which were located at the throat area of the piston bowl. The average temperatures at the throat area of the piston bowl for the baseline and LGFC cases were 633 K and 615 K, respectively. Compared with the baseline, the average temperature at the central area of the piston of the LGFC was decreased by 8.15 K.

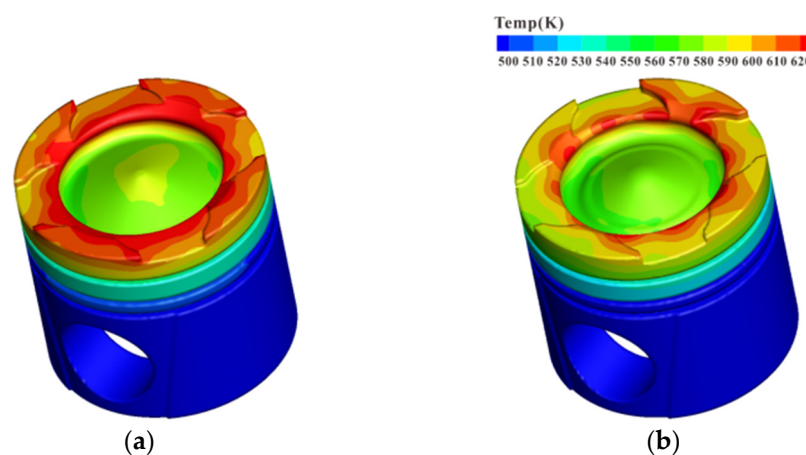


Figure 14. Temperature distribution of the piston of the baseline and LGFC. (a) Baseline. (b) LGFC.

The temperature of the piston's top surface at different distances from the piston center is shown in Figure 15. It can be seen that the temperature distributions of the baseline and LGFC were similar. The temperature increased gradually from the outer circular edge of the piston top until it reached the maximum temperature at the throat edge, i.e., the lips, of the bowl. Then, the temperature decreased steeply to the minimum value at the bottom

edge of the bowl, and increased gradually toward the center of the bowl bottom, where a small peak value was reached. Compared with the baseline, the optimized LGFC reduced the peak temperatures at the lips and bottom center of the bowl by 15–20 K.

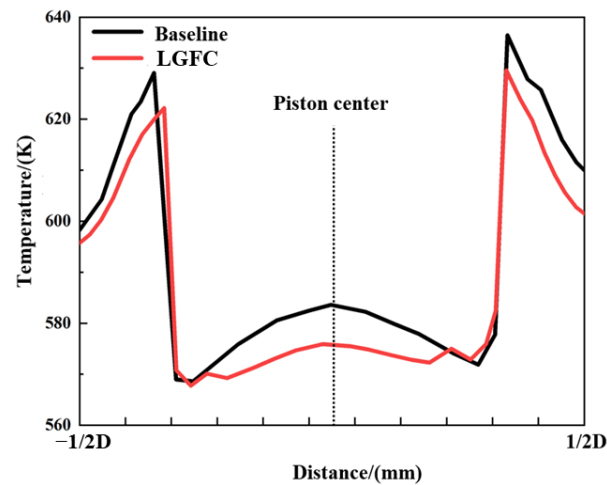


Figure 15. Temperature of the piston top surface at different distances from the piston center.

The hardness plugs were used to measure the piston head temperature under the rated power condition. The layout of the measurement point distribution is shown in Figure 16. There were six measurement points, in which the first five points were located on the top surface of the piston, and the sixth point was located on the first ring bank of the side of the piston. The point 1 and the point 5 were used to measure the temperature of the valve pockets on both sides of the piston, the point 2 was used to measure the temperature of the chamber top clearance, point 3 was used to measure the temperature of the chamber convex, point 4 was used to measure the temperature at the lip, and point 6 was used to measure the temperature of the piston backlash above the first ring bank of the piston.

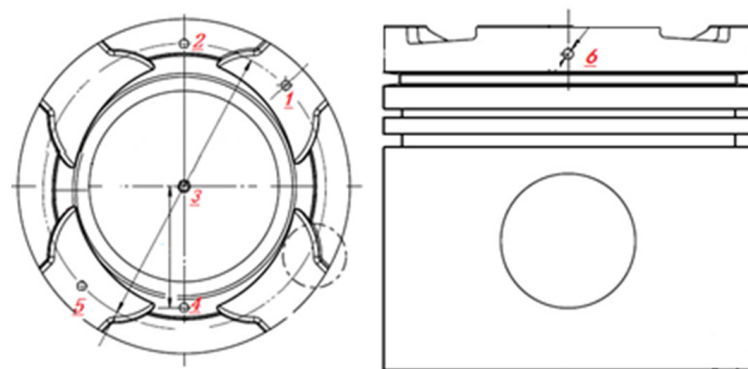


Figure 16. Location of the measuring points in the piston.

Table 5 shows the measured temperatures for both combustion chamber cases. It can be seen that all temperatures measured for the LGFC were lower than those of the baseline case. The maximum temperature occurred at point 4, and the temperature difference between the two cases was 15 K. The minimum temperature occurred at point 3, and the temperature difference between the two cases was 8 K. The temperature differences at the remaining measuring points were 15 to 24 K, showing that the LGFC combustion chamber could reduce the temperature of the piston and the heat transfer losses of the cylinder wall.

Table 5. Temperatures of the measuring points in the piston.

Measuring Point	Temperature/K (Baseline)	Temperature/K (LGFC)	Temperature Difference/K
1	612	597	15
2	650	627	23
3	537	529	8
4	668	653	15
5	637	615	22
6	649	625	24

3.2. Miller Cycle Analysis

Fuel spray dispersed the fuel particles, greatly increased the surface area of the liquid, accelerated the fuel/air mixing, and improved combustion [29–31]. The quality of the fuel spray directly affected the performance of the diesel engine. Figure 17 shows the fuel concentration distribution (fuel–air equivalent ratio) of the baseline and Miller cycle in the cylinder. It is shown that the fuel concentration distributions under different conditions schemes were generally similar. However, the high concentration area of the baseline was larger than that of the Miller cycle at TDC; the results indicate that the fuel spray diffusion rate under the Baseline condition was slightly faster, which was due to the higher temperature in the cylinder, and promoted the evaporation speed of fuel. The “high-temperature zone” of the Miller cycle reduced significantly at 20° CA ATDC, which indicated that the Miller cycle had a significant effect on reducing the combustion temperature and suppressing post-combustion.

Figure 18 shows the heat release rate of the baseline IVC timing and LIVC Miller cycle timing. According to Figure 18, the heat release rate of the Miller cycle was faster than that of the baseline during the main combustion phase of 0–25° CA ATDC, although the SOC was slightly delayed. The reason for this phenomenon is the improved fuel/air mixture with the delayed IVC of the Miller cycle, and the ignition delay was extended as the pressure and temperature at the end of compression decreased as a result of the increasing of accumulated fuel during the ignition delay period. But in the early stage of the combustion process, the heat release rate of the Miller cycle was faster, which was caused by the high velocity of the air flow in the cylinder, the combustion process was faster, and the post-combustion was restrained. Figure 19 shows the temperature distribution of the baseline and Miller cycle in the cylinder. It shows that the temperature in the cylinder under the Miller cycle was slightly lower than that of the baseline at 10° CA BTDC, which was caused by the decreased ECR and the depressed temperature at the end of the compression stroke. However, when the piston moved to TDC, the average temperature of the cylinder reached 900 K and the combustion was already started, a large amount of the fuel–air mixture accumulated during the ignition delay period, the combustion rate of the main combustion period proceeded more quickly under the Miller cycle, and the injection surface exhibited a “high-temperature zone”, with a temperature of over 2000 K. With the penetration of the spray, wall combustion appeared in the throat area and the bottom of the combustion chamber after TDC. Compared with the baseline, the “high-temperature zone” under the Miller cycle was obviously smaller; this also shows that the combustion temperature could be reduced obviously under the Miller cycle.

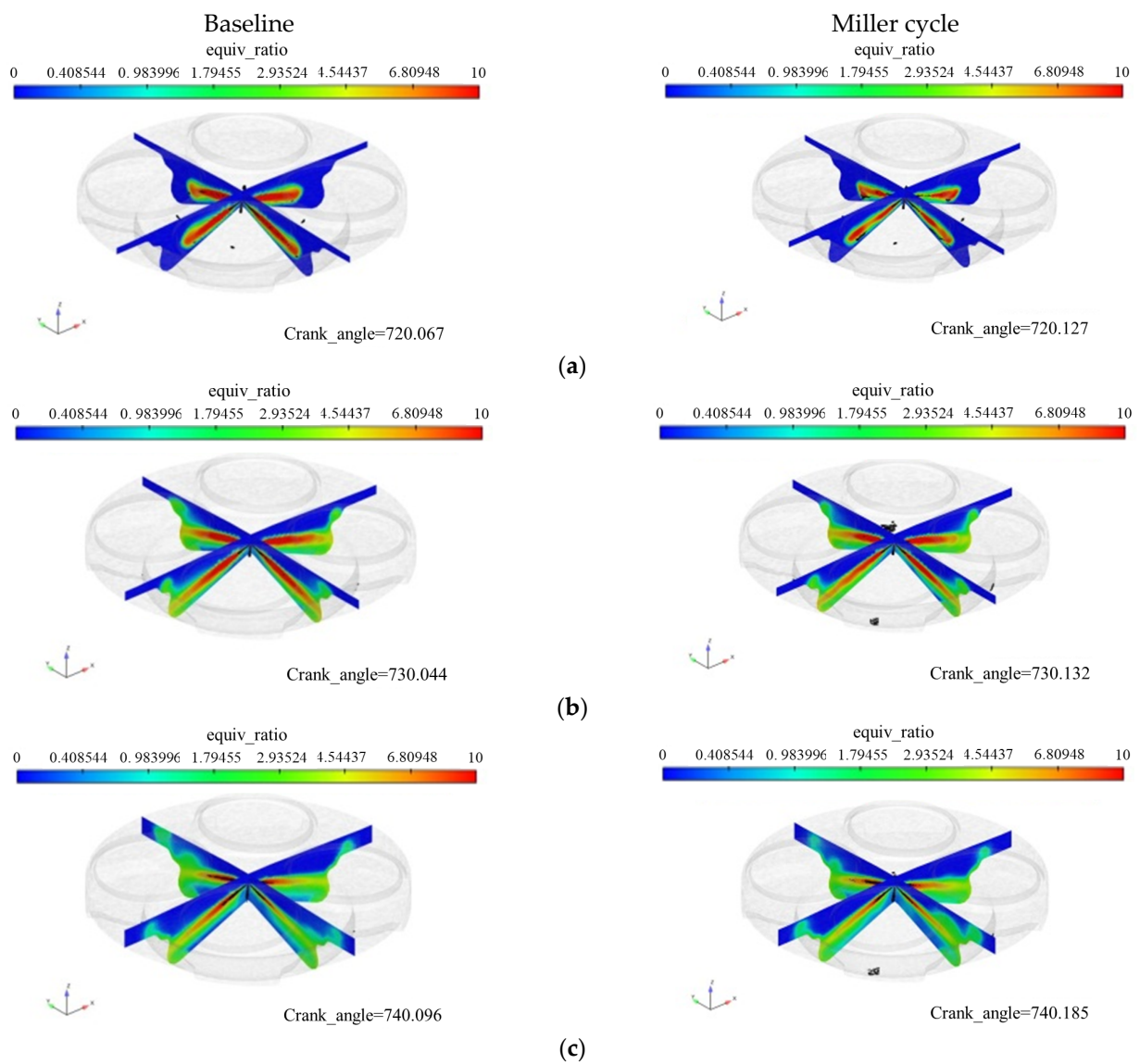


Figure 17. Fuel concentration distribution of the baseline and Miller cycle. (a) TDC. (b) 10° CA ATDC. (c) 20° CA ATDC.

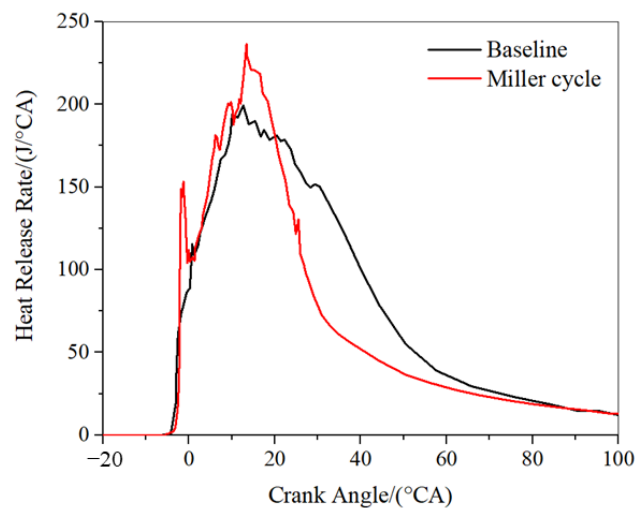


Figure 18. Heat release rate of the baseline and Miller cycle.

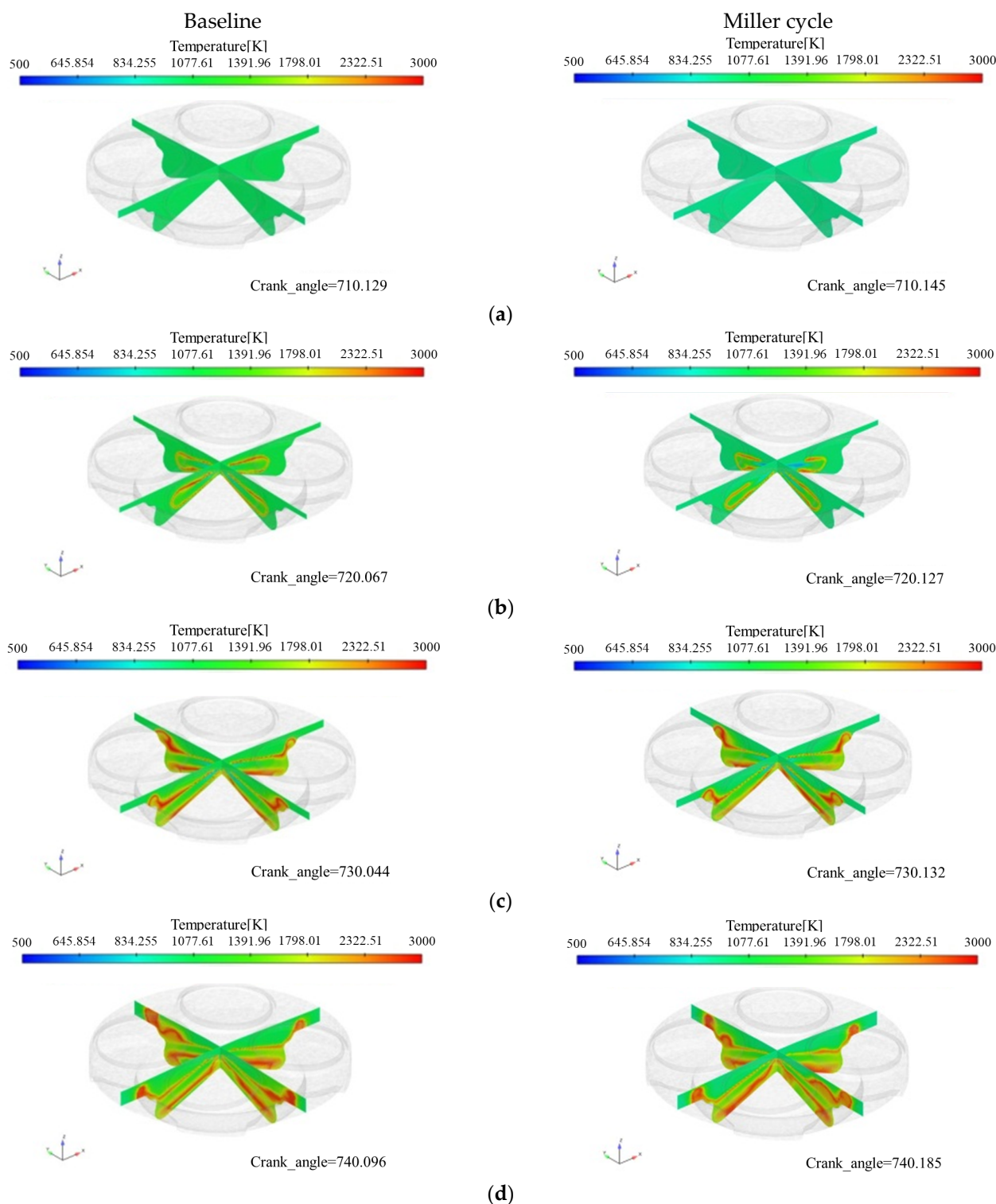


Figure 19. Temperature distribution of the baseline and Miller cycle in the cylinder. (a) 10° CA BTDC. (b) TDC. (c) 10° CA ATDC. (d) 20° CA ATDC.

As shown in Figure 20, the in-cylinder temperature decreased significantly with the maximum combustion temperature decreasing by about 45 K, which was helpful for the suppression of the in-cylinder heat load by the Miller cycle. The combustion characteristics were explored by an engine test, with a certain excess air coefficient; as the IVC was slowed to the Miller cycle timing, the indicated fuel consumption rate decreased from 218 g/(kW·h) under the baseline condition to 215 g/(kW·h) under the Miller cycle condition, indicating

that the thermal efficiency was increased by 1.4%. There may be two reasons for these results. On one hand, the pumping loss decreased under the Miller cycle condition. On the other hand, the compression pressure line decreased significantly with the Miller cycle, while the expansion pressure line decreased less (due to the low combustion temperature and the reduced heat transfer loss of the wall); thus, there was increasing effective work in the high-pressure cycle. The reduction in exhaust temperature reduced the exhaust heat loss of the whole cycle.

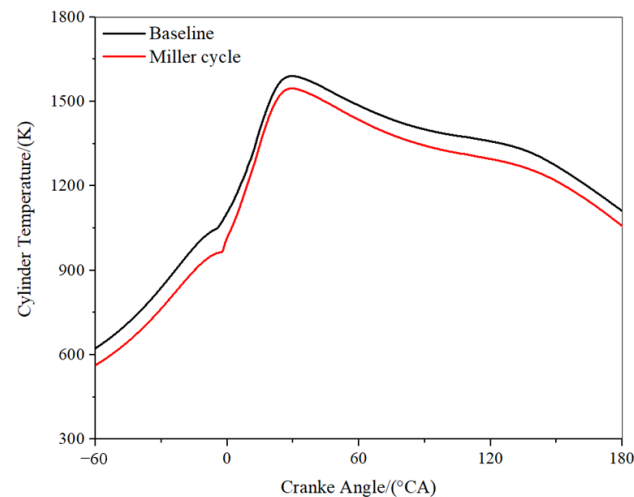


Figure 20. Average temperatures of Baseline and Miller cycle in cylinder.

As shown in Figure 21, the pumping mean effective pressure (PMEP) was negative, indicating that the pumping work of the gas exchange process under the baseline condition was also negative. But with the delay in the IVC in the Miller cycle, in order to ensure sufficient fresh intake air mass flow, the inlet pressure had to be increased, leading to an increase in the PMEP and positive pumping work, and a decrease in the fuel consumption rate.

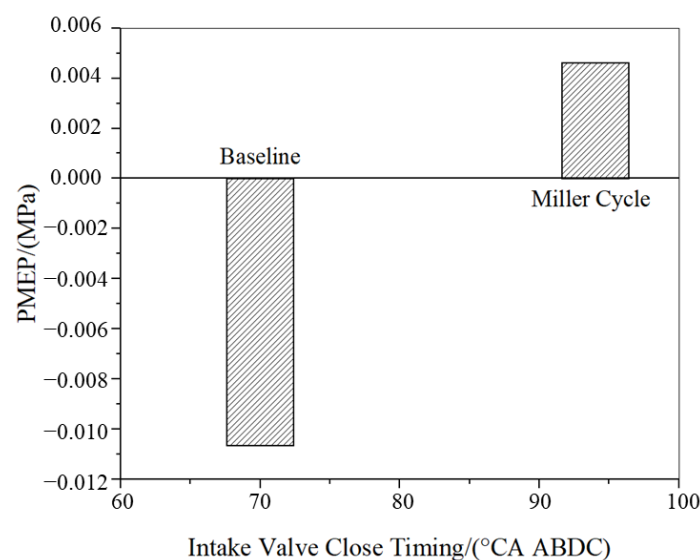


Figure 21. Pump mean effective pressure of the baseline and Miller cycle.

3.3. Combination of LGFC and Miller Cycle

To deeply understand the effect of the LGFC, Miller cycle, and the combination of the two methods, the energy balance based on the total input fuel energy was analyzed. The indicated work, combustion loss, exhaust loss, and heat transfer loss were separated from

the total conversion work of the input fuel energy according to the calculation formulas given in reference [7,32,33].

As shown in Figure 22, due to the low excess air ratio and high engine speed under the rated operating conditions, the combustion efficiency was low and the combustion loss was large. The heat insulation coating of the walls of the combustion chamber (such as the top surface of the piston) reduced the heat transfer loss, and the high engine speed further reduced the proportion of heat transfer loss of the engine; the comprehensive effect caused a lower proportion of heat transfer loss of the engine. This also shows that the LGFC or Miller cycle could reduce the exhaust loss and the combustion loss, thus increasing the proportion of the indicated work. The combination of the LGFC and Miller cycle could increase the indicated work because the exhaust loss decreased obviously.

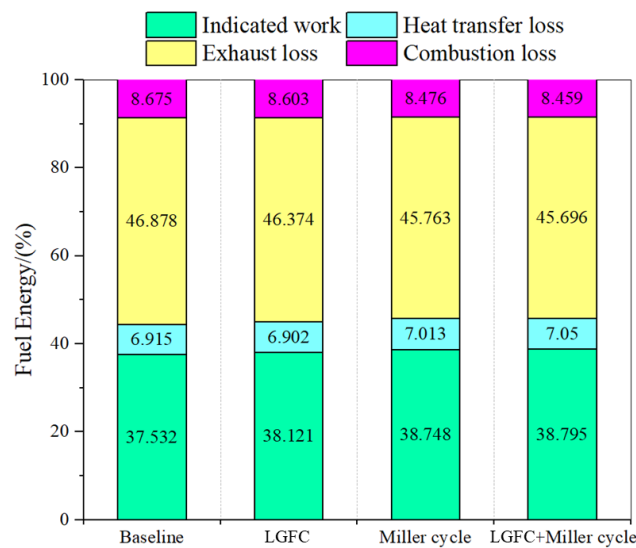


Figure 22. Energy balance analysis of different conditions.

Figure 23 shows the heat release rate of the baseline and the combination of the LGFC and Miller cycle. Compared with the baseline, the combination of LGFC and Miller cycle increased the combustion speed and notably decreased the post-combustion.

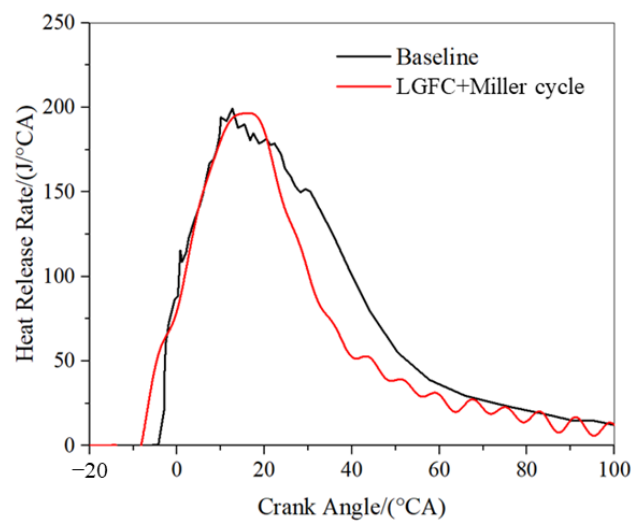


Figure 23. Heat release rate of the baseline and LGFC + Miller cycle.

The effect of the combustion chamber was studied under the rated condition with an engine speed of 3800 r/min and IMEP of 3 MPa by an experiment, and the results showed that the combined effect significantly improved the thermal efficiency of the

highly intensified diesel engine; under the combination of the LGFC and Miller cycle, the indicated specific fuel consumption decreased from 220.5 g/(kW·h) to 209.7 g/(kW·h), and the thermal efficiency of the working process was 2.1% higher than that of the baseline.

4. Conclusions

To improve the thermal efficiency of a highly intensified diesel engine, the effect of combustion chamber geometry parameters (including the lip radius, lip depth, bowl radius, and bowl distance) and Miller cycle (LIVC) were analyzed. Based on the experiment and simulation, the LGFC, Miller cycle, and the combination of two methods were discussed. The main conclusions are summarized as follows:

1. The simulated results show that, in the LGFC combustion system, the quality of the fuel/air mixture increased in the central area of the combustion chamber and the temperature gradient of the cross-section from the cylinder center to the cylinder wall decreased. Large-scale flow easily formed in the cavity of the chamber due to the large longitudinal space area, and the fuel distribution in the cylinder was concentrated in the longitudinal direction, along with the movement of the piston. The combustion was more concentrated in the pit, the combustion on the outside area of the piston top surface decreased, the start of combustion was earlier, the combustion process became more concentrated, and the post-combustion decreased slightly;
2. The experimental and simulated results show that, compared with the temperatures of the baseline, the LGFC piston could reduce the average temperature of the piston top by about 3% and depress the heat transfer losses of cylinder walls;
3. At a certain excess air coefficient, the indicated specific fuel consumption decreased. The compression pressure line decreased significantly in the Miller cycle, while the expansion pressure line decreased less, and there was an increase in effective work in the high-pressure cycle. The PMEP increased by about 0.015 MPa and the pump work became positive under the Miller cycle condition.
4. Under the combination of the LGFC and Miller cycle condition, the effect significantly improved the thermal efficiency of the highly intensified diesel engine and the thermal efficiency of the working process was 2.1% higher than that of the baseline.

Author Contributions: Conceptualization, Y.A.; Methodology, Z.W. and J.L.; Validation, C.H. and R.M.; Formal analysis, Y.L. and R.C.; Investigation, Z.W.; Resources, Y.L. and C.H.; Data curation, Y.L. and Y.A.; Writing—original draft, Z.W.; Writing—review & editing, Y.L., J.L., R.C. and Y.A.; Visualization, R.C. and R.M. All authors have read and agreed to the published version of the manuscript.

Funding: This research was funded by National Natural Science Foundation of China grant number 51476151.

Institutional Review Board Statement: Not applicable.

Informed Consent Statement: Not applicable.

Data Availability Statement: The authors confirm that the data supporting the findings of this study are available within the article.

Acknowledgments: This work was supported by financial support from the National Natural Science Foundation of China grant number 51476151.

Conflicts of Interest: The authors declare no conflict of interest.

References

1. Steinparzer, F.; Nefischer, P.; Hiemesch, D.; Kaufmann, M. The new BMW six-cylinder top engine with innovative turbocharging concept. *MTZ* **2016**, *71*, 38–44. [[CrossRef](#)]
2. Heiduk, T.; Weiß, U.; Frohlich, A.; Helbig, J. The new V8 TDI engine from Audi. *MTZ* **2016**, *77*, 20–25.
3. Eichler, F.; Demmelbauer-Ebner, W.; Strobel, J.; Kühlmeyer, J. The new W12-TSI engine of the Volkswagen group. *MTZ* **2016**, *77*, 16–23. [[CrossRef](#)]

4. Lamping, M.; Korfer, T.; Wix, K. HSDI Diesel Engines—FEV's high power density concepts. *ATZ Autotechnol.* **2006**, *9*, 40–45. [[CrossRef](#)]
5. Pesce, F.C.; Vassallo, A.; Beartice, C.; Di Blasio, G. Exceeding 100 kW/L Milestone: The next step towards defining high performance diesel engines. In Proceedings of the 25th Aachen Colloquium Automobile and Engine Technology 2016, Aachen, Germany, 10–12 October 2016; pp. 159–184.
6. Demark, R.; Groddeck, M.; Ruetz, G. The new diesel engines series 890 by MTU. *MTZ Worldw.* **2006**, *67*, 2–5. [[CrossRef](#)]
7. Hao, C.; Zhang, Z.; Wang, Z.; Bai, H.; Li, Y.; Li, Y.; Lu, Z. Investigation of spray angle and combustion chamber geometry to improve combustion performance at full load on a heavy-duty diesel engine using genetic algorithm. *Energy Convers. Manag.* **2022**, *267*, 115862. [[CrossRef](#)]
8. Chen, Y.; Li, X.; Li, X.; Zhao, W.; Liu, F. Verifying the all-flow-guided assumption of the lateral swirl combustion system in DI diesel engines. *Fuel* **2020**, *266*, 117079. [[CrossRef](#)]
9. Li, X.; Qiao, Z.; Su, L.; Li, X.; Liu, F. The combustion and emission characteristics of a multi-swirl combustion system in a DI diesel engine. *Appl. Therm. Eng.* **2017**, *115*, 1203–1212. [[CrossRef](#)]
10. Su, L.; Li, X.; Zhang, Z.; Liu, F. Numerical analysis on the combustion and emission characteristics of forced swirl combustion system for DI diesel engines. *Energy Convers Manag.* **2014**, *86*, 20–27. [[CrossRef](#)]
11. Lu, F.; Yu, X.; Zhang, Y.; Han, S.; Fang, Y. Available energy analysis method and experiment investigation on energy-saving potential for vehicle diesel engine. *Chin. Intern. Combust. Engine Eng.* **2012**, *33*, 61–66.
12. Zhao, C.; Yue, Y.; Zhou, L.; Zhang, F. Thermodynamic analysis of diesel engine 6V150. *Trans. Beijing Inst. Technol.* **2004**, *24*, 500–503.
13. Dahlstrom, J.; Andersson, O.; Tuner, M. *Experimental Comparison of Heat Losses in Stepped-Lip Bowl and Re-Entrant Combustion Chambers in a Light Duty Diesel Engine*; SAE Technical Paper Series 2016-01-0732; Society of Automotive Engineers: Warrendale, PA, USA, 2016.
14. Ehleskog, M.; Gijrja, S.; Denbratt, I. *Effects of Variable Inlet Valve Timing and Swirl Ratio on Combustion and Emissions in a Heavy-Duty Diesel Engine*; SAE Technical Paper Series 2012-01-1719; Society of Automotive Engineers: Warrendale, PA, USA, 2012.
15. Theißl, H.; Kraxner, T.; Seitz, H.; Kislinger, P. Miller valve timing for future commercial diesel engines. *MTZ* **2015**, *76*, 5–11.
16. Chen, B.; Zhang, L.; Luo, Q.; Zhang, Q. The thermodynamic analysis of an electrically supercharged Miller cycle gasoline engine with early intake valve closing. *Sādhanā* **2019**, *44*, 65. [[CrossRef](#)]
17. Ortwin, D.; Schutting, E.; Eichlleder, H. Extended expansion linkage engine: A concept to increase the efficiency. *Automot. Engine Technol.* **2018**, *3*, 83–92.
18. Wei, S.; Zhao, X.; Liu, X.; Qu, X.; He, C.; Leng, X. Research on effects of early intake valve closure (EIVC) miller cycle on combustion and emissions of marine diesel engines at medium and low loads. *Energy* **2019**, *173*, 48–58. [[CrossRef](#)]
19. Zhang, Y.; Wang, Z.; Bai, H.; Guo, C.; Liu, J.; Li, Y. *The Reduction of Mechanical and Thermal Loads in a High-Speed HD Diesel Engine Using Miller Cycle with Late Intake Valve Closing*; SAE Technical Paper Series 2017-01-0637; Society of Automotive Engineers: Warrendale, PA, USA, 2017.
20. Long, L.; Jianhua, H.; Zhiguo, Y. The optimization on effective thermal efficiency of low-speed diesel engine. *SHIP Eng.* **2019**, *41* (Suppl. 1), 218–225.
21. Nevin, R.; Sun, Y.; Gonzalez, D.; Reitz, R. *PCCI Investigation Using Variable Intake Valve Closing in a Heavy-Duty Diesel Engine*; SAE Technical Paper Series 2007-01-0903; Society of Automotive Engineers: Warrendale, PA, USA, 2007.
22. Millo, F.; Mallamo, F.; Mego, G. *The Potential of Dual Stage Turbocharging and Miller Cycle for HD Diesel Engines*; SAE Technical Paper Series 2005-01-0221; Society of Automotive Engineers: Warrendale, PA, USA, 2005.
23. Kovacs, D.; Eilts, P. *Potentials of the Miller Cycle on HD Diesel Engines Regarding Performance Increase and Reduction of Emissions*; SAE Technical Paper Series 2015-24-2440; Society of Automotive Engineers: Warrendale, PA, USA, 2015.
24. Wang, Z.; Zhang, Y.; Wang, L.; Liu, J.; Bai, H.; Li, Y. Effect of LIVC Miller cycle on combustion and gas exchange on a highly intensified single-cylinder diesel engine. *Acta Armamentarii* **2019**, *40*, 8–18.
25. Han, Z.; Reitz, R.D. Turbulence modeling of internal combustion engines using RNG κ - ϵ models. *Combust Sci Technol* **1995**, *106*, 267–295. [[CrossRef](#)]
26. Liu, A.B.; Mather, D.; Reitz, R.D. *Modeling the Effects of Drop Drag and Breakup on Fuel Sprays*; SAE Technical Paper Series 930072; Society of Automotive Engineers: Warrendale, PA, USA, 1993.
27. Lu, Y.H.; Zhang, X.; Xiang, P.L.; Dong, D. Analysis of thermal temperature fields and thermal stress under steady temperature field of diesel engine piston. *Appl. Therm. Eng.* **2017**, *113*, 796–812. [[CrossRef](#)]
28. Deng, X.; Lei, J.; Wen, J.; Wen, Z.; Shen, L. Multi-objective optimization of cooling galleries inside pistons of a diesel engine. *Appl. Therm. Eng.* **2018**, *132*, 441–449. [[CrossRef](#)]
29. Park, S.; Reitz, R. Optimization of fuel/air mixture formation for stoichiometric diesel combustion using a 2-spray-angle group-hole nozzle. *Fuel* **2009**, *88*, 843–852. [[CrossRef](#)]
30. Mobasher, R.; Peng, Z. *A Computational Investigation into the Effects of Included Spray Angle on Heavy-Duty Diesel Engine Operating Parameters*; SAE Technical Paper 2012-01-1714; Society of Automotive Engineers: Warrendale, PA, USA, 2012.
31. Sener, R.; Yangaz, M.; Gul, M.Z. Effects of injection strategy and combustion chamber modification on a single-cylinder diesel engine. *Fuel* **2020**, *266*, 117122. [[CrossRef](#)]

32. Kokjohn, S.; Hanson, R.; Splitter, D.; Reitz, R.D. Fuel reactivity controlled compression ignition (RCCI): A pathway to controlled high-efficiency clean combustion. *Int. J. Engine Res.* **2011**, *12*, 209–226. [[CrossRef](#)]
33. Yao, Z.; Qian, Z.; Li, R. Energy efficiency analysis of marine high-powered medium speed diesel engine base on energy balance and exergy. *Energy* **2019**, *176*, 991–1006. [[CrossRef](#)]

Disclaimer/Publisher’s Note: The statements, opinions and data contained in all publications are solely those of the individual author(s) and contributor(s) and not of MDPI and/or the editor(s). MDPI and/or the editor(s) disclaim responsibility for any injury to people or property resulting from any ideas, methods, instructions or products referred to in the content.